High capacity chipless RFID tags for biomass tracking application

Amjad Ali[1] , Christopher Smartt[1], Ed Lester[2], Orla Williams[2]
and Steve Greedy[1]

[1]School of Electrical Engineering, University of Nottingham, Nottingham, UK and [2]Advanced Materials Research Group, Faculty of Engineering, University of Nottingham, Nottingham, UK

Abstract

The design of a low-cost, flexible, miniaturized, and a high code density chipless radio-frequency identification (RFID) tag is presented as a solution for tracking the transportation of biomass fuel pellets. The performance of the tag is presented and demonstrates the applicability of the design for different material systems, while maintaining a compact size of 5.06 cm^2. The tag consists of nested concentric hexagonal elements and a central spiral resonator suitable for ID encoding. The tag presented demonstrates code density of 3.6-bits/cm^2, possesses angular stability up to 60°, and high radar cross section (RCS). The tag performance was also observed for tracking 5 kg of fly-ash biomass. Additionally, as the tag mass mostly consists of FR4, PET, or Taconic TLX-0 with a minute mass of either copper, gold, or silver, the tag can be easily combusted and disposed of during biomass combustion. The novel features of this tag are the combination of hexagonal and spiral shape slots for maximum space utilization thereby achieving high RCS signatures along with high code density. All these properties of the proposed chipless RFID tag provide a pioneering pathway for a real-time biomass tracking application.

Introduction

Electricity generation from renewables accounted for 33% of all electricity produced in the UK in 2018 [1]. Bioenergy represented 31.6% of the renewable energy produced, with plant-based biomass producing 23 TWh of electricity in the UK in 2018, primarily via converted coal-fired pulverized fuel power stations. In the UK alone, 7.2 million tons of biomass were used to produce electricity in 2018, with 7.8 million tons of wood pellets being imported, 82% originating from the USA or Canada [2]. Different types of biomass production, supply chain to end user, and storage are shown in Fig. 1 [3]. Biomass pellet transportation and storage is known to suffer from self-heating and self-ignition due to anaerobic respiration, which is linked to atmospheric conditions the material is being stored in [4]. The self-heating of materials leads to the decomposition of the material, formation of spores and fungus, and the release of flammable gases [5]. This can lead to fires and explosions in several parts of the biomass supply chain [6, 7]. Currently there are no commercially economical methods of monitoring the whole life cycle physical conditions inside large volumes of biomass in storage. Due to fire risks, sensors cannot have batteries and it is difficult to recover sensors before combustion. Thus, any whole life monitoring system must minimize the risk of fire, not pose a blocking hazard, be combustible, while also being low cost to produce. To date, no such sensor tag has been demonstrated.

A radio-frequency identification (RFID) tag is a wireless data-capturing device that utilizes radio frequency (RF) signal power for recognition of remotely located objects. It has various advantages over barcode technology [8, 9], such as long-read range, no need for line-of-sight detections, and automatic identification.

RFID technology is emerging in auto-tracking systems, commerce, health monitoring systems, security, access control, and other industries due to their low cost, simple design, and realization [8]. It is anticipated that in the near future over a billion items will be using RFID technology for automatic monitoring [10]. The use of RFID tags for auto-tracking has already been established; for example active RFID tags have been used successfully to track the movement of goods across the globe [11, 12]. In this application, the tags rely on their own local/internal power source to function and can therefore be considered a risk in an environment where sources of possible ignition need to be avoided. In addition, active tags add additional cost and bulk and are less environmentally friendly than their passive counterparts.

In this work, we propose a passive chipless RFID tag for tracking and monitoring biomass pellet life cycle; from production to transportation and their subsequent use as a fuel in power stations. The proposed tags are suitable for location within the biomass pellet stock and can be read by RFID readers at suitable points in the transport. Being passive, the tags pose no risk as a source of ignition, they can be considered as disposable items and the material systems proposed can be combusted with the biomass fuel to produce electricity.
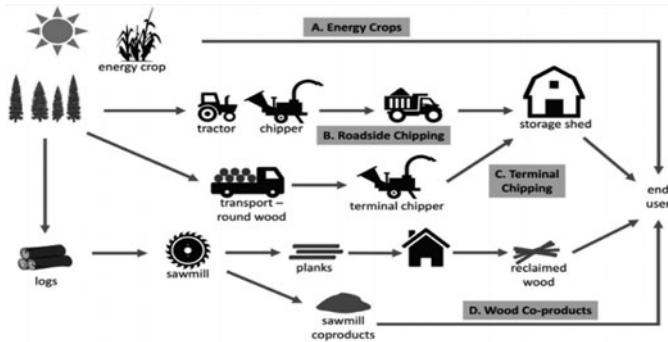
Fig. 1. Woody biomass and energy crop straws supply chain to end user [3].

As already mentioned there are two existing RFID technologies for such applications [13], active and passive RFID tags. Active RFID tags are powered through an on-board battery and are typically used where long read ranges are required [13]. However, the cost of active tags is high due to costs associated with the battery and the associated additional complexity of the tag design. This high cost makes active tags unattractive for bulk tracking/monitoring applications [10], and a passive RFID solution is preferred which has been the subject of much research studies [14]. Furthermore, the omission of batteries minimizes the fire risk in biomass transport, storage, and milling applications, and means that tags are more likely to be ATEX-rated [15, 16]. Thus, the tag can be used as a single use tracking device which can be comminuted and combusted with the biomass pellets in pulverized fuel boilers. Passive RFID tag-based systems utilize a tag reader to provide power by directing a source of electromagnetic (EM) energy at the tag [17]. An antenna system on the tag collects this energy and then transmits data back to the reader, either as energy simply reflected by the antenna or as a transmission encoded by an integrated chip (IC) within the tag. Therefore, passive tags may be categorized into chip-based and chipless RFID tags [10].

Chip-based tags consist of an antenna responsible for collecting power, transmitted by the tag reader, which is connected to an IC. The received signal energizes the chip which then transmits back the stored data to the reader receiver according to specific standards [17]. A number of various chip-based RFID tags and their readers are shown in Fig. 2(a). These chip-based passive tags, RFMICRON, are more suitable for non-metallic surface tracking and sensing applications such as humidity and temperature sensing. The readers used for reading the data of these tags are shown in Figs 2(b) and 2(c). The reader in Fig. 2(c), Thing-Magic is a development kit, which could read a tag's identity along with, for example, temperature or other sensing capability. The reader in Fig. 2(b), qIDmini, is a handheld reader which could read tag's identity only and store it in its memory. The stored identities could be transferred to a computer or a hub-point. These tags were readable up to 8-m distance in the lab, at the University of Nottingham. Chip-based tags allow for a relatively high storage data, display high gain and allow for relatively long read ranges, up to 8 m, and better environmental sensing capabilities at the cost of complex: design, fabrication, and IC integration. This functionality makes these tags expensive and presents barriers to their use in bulk quantity applications, such as warehouse inventory management systems [17]. Therefore, significant research efforts have been made to reduce the cost and

complexity of the unit tags, by providing the necessary information without a storage unit (IC), which has resulted in the development of chipless RFID tags [18].

Chipless RFID tags are simple in their design, inexpensive to produce, and are easier to reduce in size albeit with a resulting loss in code capacity, and read range as compared to chip-based RFID tags [19]. In presenting the advantages offered by differing tag design, the disadvantages are often not presented, and they are noted thus:

- The tags in [8, 18–23] are large in size and result in low code density.
- The tags in [22–26] have weak backscattered signatures and so are susceptible to disruption by noise, where the reader is unable to distinguish between data and background noise.
- The angular stability, i.e., the ability of the reader to collect the data over a range of angles of incidence to the tag was discussed only in [27]. However, the spectral signature was stable up to 30°. For further increase in the angle of incidence a significant reduction in magnitude of the reflected signal and a spectral shift was observed.

This work presents a chipless tag design with a code density of 3.6-bits/cm^2 operating in the frequency range 1.5–15 GHz. Furthermore, the tag displays excellent angular stability, inexpensive to produce, and suitable for miniaturization. The tag is designed to be readable in the far-field region that which equates to distances >1 m and at distances of up to 3 m. The tag uses a unique nested concentric hexagonal and spiral geometry as the reflecting element, providing up to 2^{18} individual IDs. The hexagonal elements are nested concentrically to decrease the overall size of the tag, while improving code density. The following features have been significantly improved to increase the performance of the suggested tag:
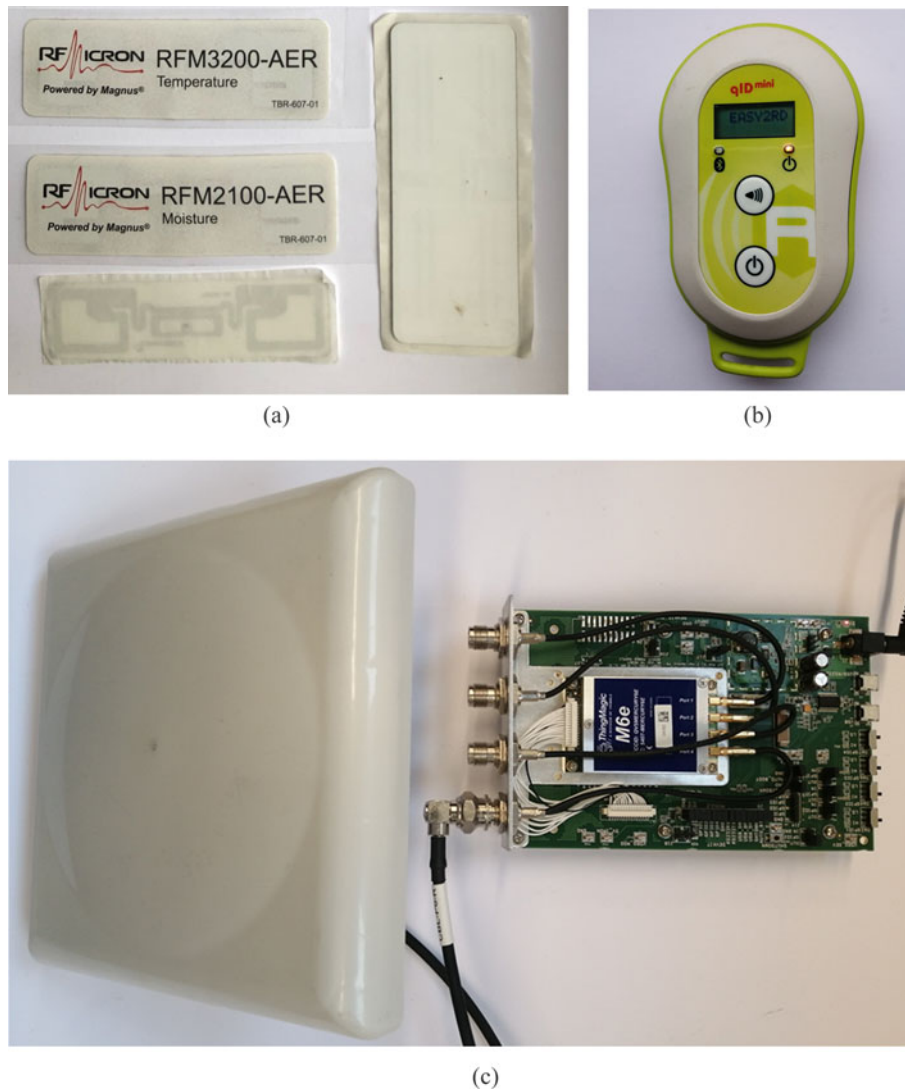
- Angular stability is ensured for θ and Φ up to 60° as compared to [8, 13, 14, 17, 20, 21, 23, 28–33].
- Spectral signature nulls used for data encoding achieved a minimum magnitude of 5 and a maximum magnitude of 22 dBsm as compared to [22, 26, 30].

Although a number of high code density tags have been previously reported, their radar cross section (RCS) signature is either very low (<5 dBsm) or even lower (below 35 dBsm) [22, 26, 30]. If the signature magnitude is <5 dBsm, then the signatures are very susceptible to either being canceled out by noise or not being detectable at all during real-time measurements. The tag proposed in this study demonstrated and maintained a high magnitude RCS, making it practical for biomass applications where the biomass results in significant scattering of the incident/reflected signal as we show that the tag response could still be detected in such a scenario. The high code density and low manufacturing costs of the tag therefore make it suitable for biomass tracking throughout all stages of the biomass lifecycle.

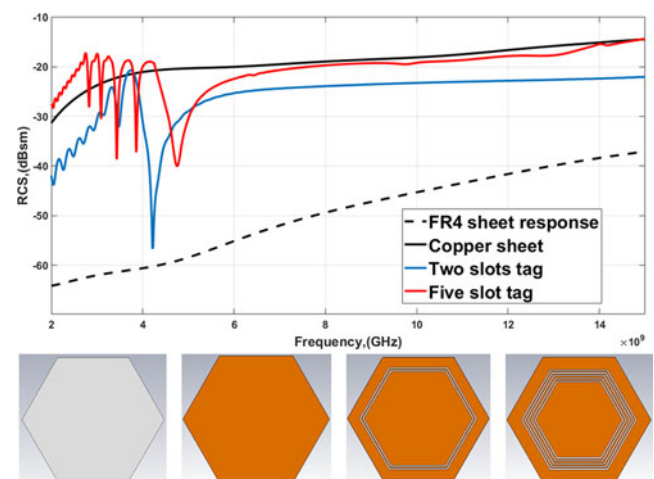## Design and operation of passive RFID tag

Tag geometry and design

A chipless RFID tag's data encoding is achieved by varying the tag's reflected spectral signature through a specific arrangement of RF scatterers and resonators on the tag. Closed-loop [14],

Fig. 2. (a) Various active and passive RFID tags having large size, complex design, and high cost, (b) qIDmini reader, and (c) Thing-Magic RFID reader.

rectangular split ring [18], rectangular slot [34], metal strip [21], circular split ring [22], spiral resonators [20], circular loop [28], and C-shaped [28, 29] are commonly reported resonators used in chipless RFID tags for encoding data IDs. The proposed tag consists of an arrangement of nested concentric hexagonal and spiral-shaped resonant structures. Hexagonal shape resonators were selected due to their space efficiency, maximum angular stability, and minimum mutual coupling which results in minimum noise and high code density as compared to those already described in the literature [32, 34]. The resonators were etched into a 0.035 mm thick copper cladding layer on an FR4 substrate, with a substrate thickness of 1.6 mm, dielectric permittivity $\epsilon_r = 4.7$ and 0.019 tangent loss.
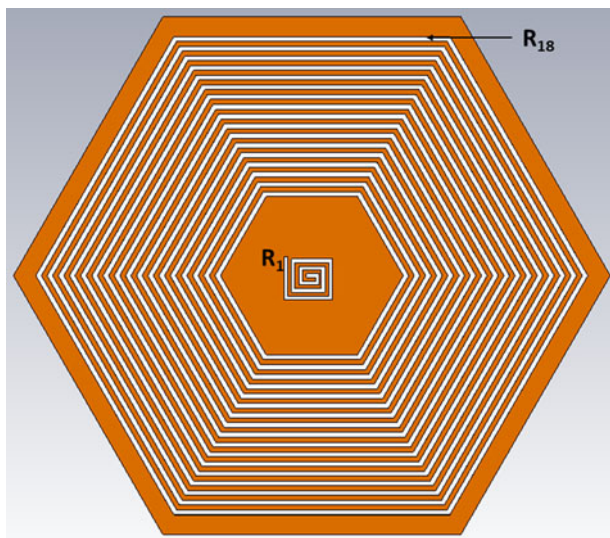
Equation (1) was used to determine the radius R_s of the hexagonal resonator for a desired resonant frequency, f_{res}, where c is the speed of light and ε_r is the relative permittivity of the substrate used. Initially, a hexagonal-shaped FR4 and copper sheet was simulated, as shown in Fig. 3. Then equation (1) was applied to the design of tags with two and five hexagonal slots. The calculated radii of two hexagons were 8.8 and 10 mm for spectral signatures at 4.22 and 3.49 GHz, respectively as shown in Fig. 3. The simulated RCS response of two-slots tag (Fig. 3) shows that RCS nulls of magnitude 7 and 27 dBsm were achieved after

Fig. 3. Hexagonal-shaped FR4, copper sheet, two and five hexagonal-shaped slots tag with their corresponding simulated RCS response.

illuminating the two-slots tag with a plane wave. This tag is able to encode 2-bit, and the data capacity can be increased simply by adding further concentric resonant elements. This

Fig. 4. 18-bit chipless RFID tag. Hexagonal resonators (as listed in Table 1) having 0.3 mm width and gaps, along with spiral resonator (R_1 = 17.35 mm length).

approach is illustrated in Fig. 3 for the case of a 5-bit tag where the slots radii are 11.2, 10.6, 10, and 9.4 mm while a 0.3 mm gap and width were maintained. The width and gaps between slots could be narrowed as well as wider; the narrowed ones give higher code density. However, the narrowed gaps and widths of slots would be difficult from manufacturing point of view as well as from reading point of view, because the RCS reflection of very thin slot would be invisible to the receiving antenna. In contrast, the wider slots are easy to manufacture and readable but will reduce code density. Therefore, 0.3 mm is a good trade-off between higher code density, ease of manufacture, and good readability:

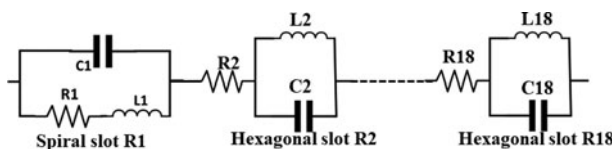$$R_s = C2\pi f_{res}\sqrt{2\varepsilon_r + 1} \qquad (1)$$

This approach was used to realize an 18-bit tag within a very compact size of 5.06 cm^2 as shown in Fig. 4. It should be noted that adding further resonators will slightly shift the resonant frequency of the adjacent structures. Therefore, care must be taken to minimize the resulting frequency shift. This shift occurs due to the mutual coupling effect. However, this effect can be controlled by optimizing the designed variables such as total tag size, radii, widths, gaps between slots and substrate height and types. The optimization process consists of calculating the resonant frequency and then repeatedly simulating the structure. During these simulations, 17 hexagonal slots were adjusted in close proximity to an area of only 2.25 × 2.25 cm^2, where each slot is separated by 0.3 mm on a hexagonal substrate of radius 16 mm. To achieve the 18th bit a spiral resonator of minimum length was used instead of a hexagonal resonator, as shown in Fig. 4. Details of the complete geometry are listed in Table 1.

Equivalent circuit model of the proposed tag

The proposed tag consists of two types of slots: one is spiral, and the other is hexagonal. The spiral slot equivalent circuit model consists of a capacitor in parallel with a series inductor and resistor. The 17 hexagonal slots equivalent circuit model consists of an

Table 1. Radius, resonating frequency, and guard band of each resonator

Resonator (Rx)	Radius (mm)	Frequency (GHz)	Guard band (GHz)
R1 (length)	17.35	12.64	0.82
R2 (radius)	4	11.82	0.82
R3	4.6	9.93	1.89
R4	5.2	8.57	1.36
R5	5.8	7.47	1.1
R6	6.4	6.6	0.87
R7	7	5.86	0.74
R8	7.6	5.21	0.65
R9	8.2	4.68	0.53
R10	8.8	4.22	0.46
R11	9.4	3.81	0.41
R12	10	3.49	0.32
R13	10.6	3.17	0.32
R14	11.2	2.89	0.28
R15	11.8	2.64	0.25
R16	12.4	2.43	0.21
R17	13	2.3	0.13
R18	13.6	2.02	0.28

Fig. 5. Equivalent circuit model of the proposed chipless RFID tag.

inductor and capacitor in parallel with the series resistor, as shown in Fig. 5. The spectral signature dips are achieved by the coupled LC resonators.

In Fig. 5, R indicates the attenuation in the ultra-wide band signal. C represents the capacitance in closely coupled slots; its value is directly proportional to the total slot length and inversely proportional to the slot width. L represents the inductance in the closely coupled metallic strips, whose value is also directly proportional to the length of the metallic strip and inversely proportional to the width of the metallic strip. In our proposed tag, the mutual capacitance and inductance values are significantly increased due to the high number of slots.

Results and discussion

Item encoding

The simulations were performed using a commercially available electromagnetic simulation suite, CST Studio by 3DS Simulia [35]. The backscattered spectral signatures are computed after illuminating the tag by a horizontal plane wave and were observed using an RCS probe placed in the far-field, at a distance of 1 m
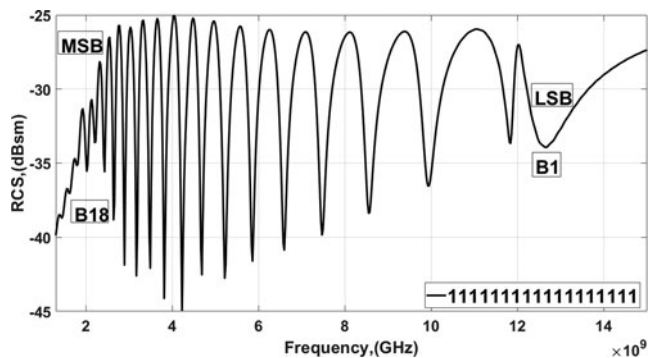
Fig. 6. 18-bit tag RCS response, bit (B1) corresponds to the resonator (R_1) and vice versa.
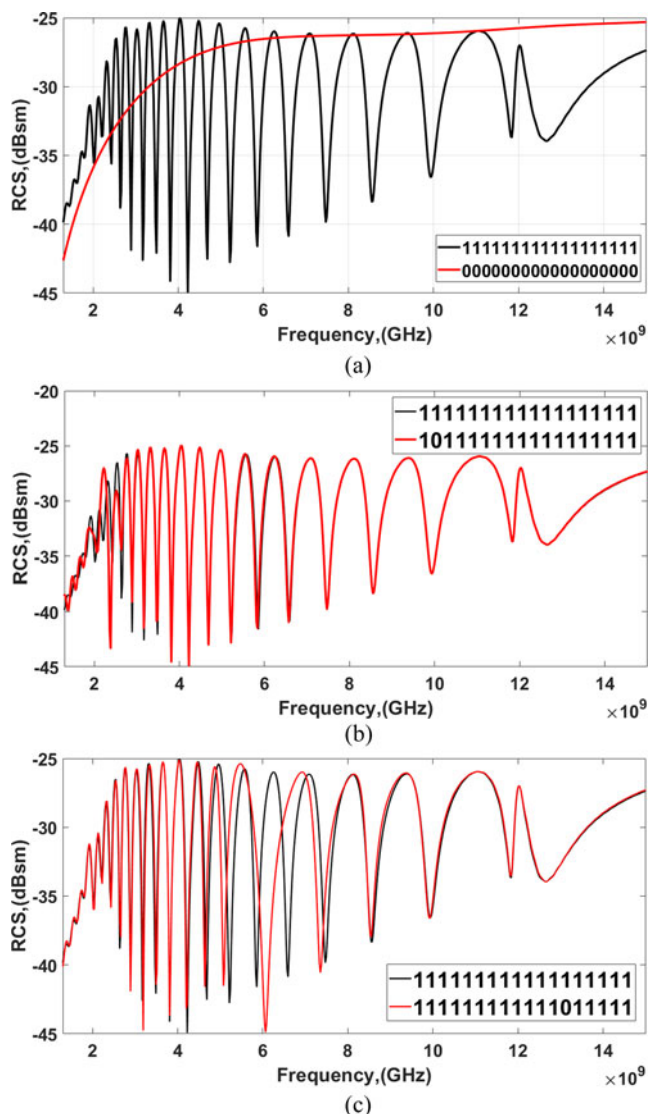

Fig. 7. Different data encoding with a minimum guard band of 0.17 GHz were achieved by removing: (a) all slots, (b) slot seventeenth, and (c) slot sixth.
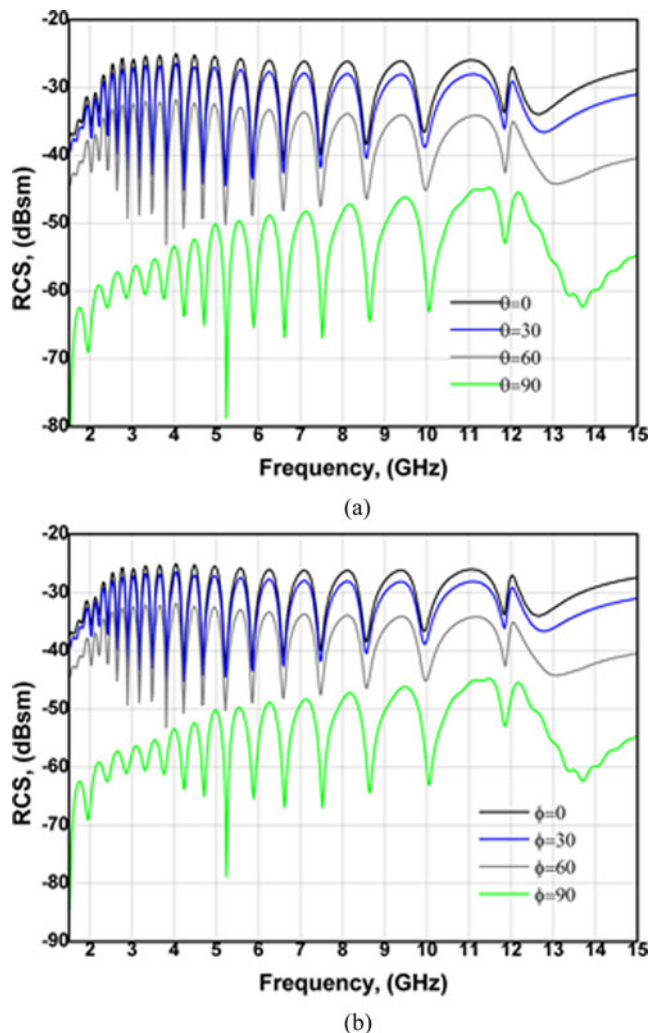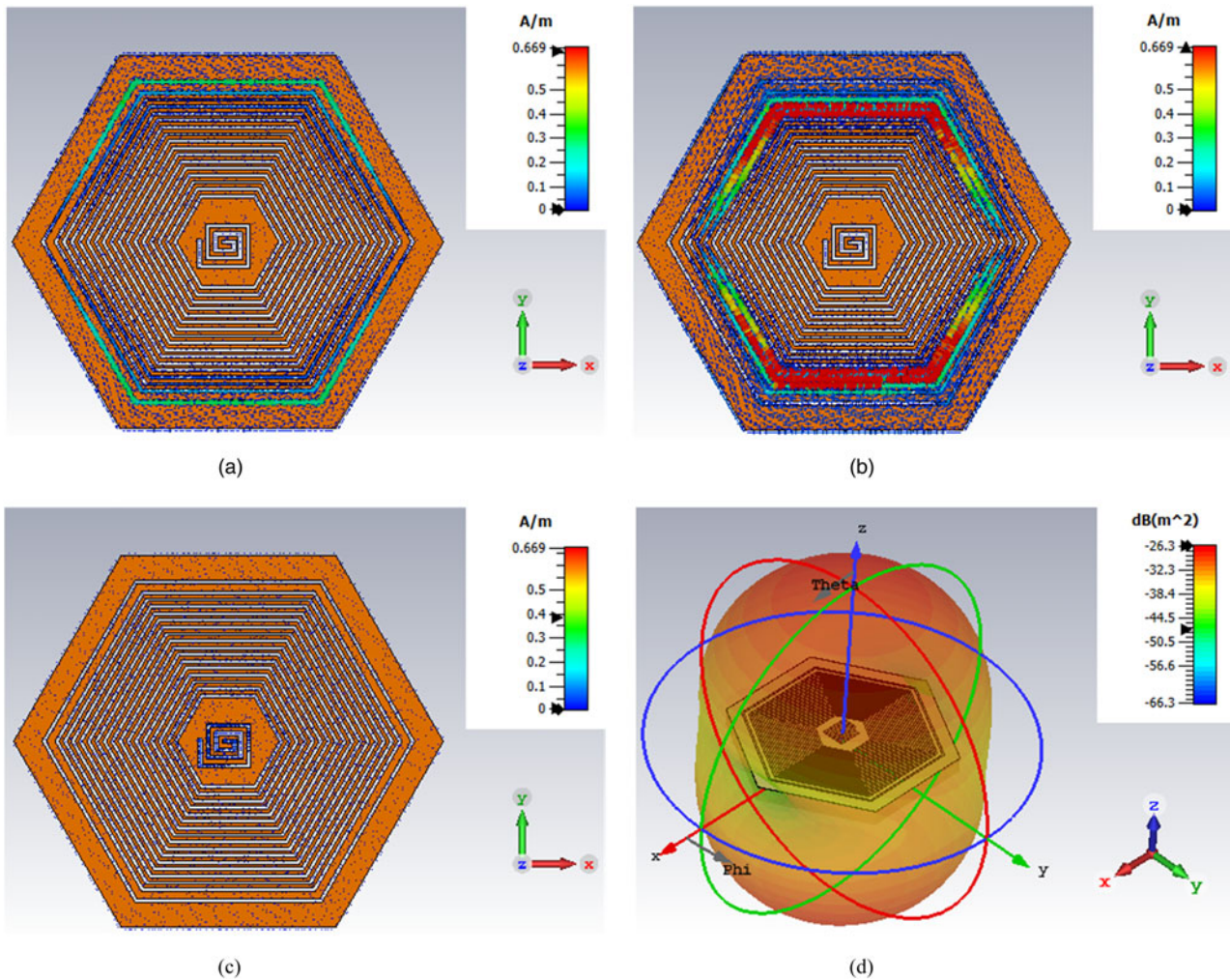

Fig. 8. Theoretical results of elevation "θ" and "Φ" angles of incidence for the proposed chipless tag.

of view, B1 and B18 were treated as the least-significant bit and most-significant bit, respectively. Each resonator gives a distinct spectral signature dip in its RCS response which is treated as data bit "1," while the absence of a resonator corresponds to a smooth curve which is treated as data bit "0." As a proof of data encoding capability, four different data combinations are presented by altering the number and sequence of resonators.

Specifically, data were encoded by the removal of resonators R_{17} and R_6, resulting in spectral signature codes of "101111111111111111" and "111111111111011111," respectively. The resulting RCS of these two cases and that of all bits present are shown in Figs 7(a)–7(c). Additionally, the tag RCS responses were simulated with different substrates, for example, Taconic TLX-0, PET, and conducting layers such as silver and gold with a difference of <5% on an average.

The sensitivity of tags to the angle of incidence of excitation was investigated, and it was observed that the spectral signatures are unaffected by incidence angles of θ-or-Φ up to 30° (Fig. 8). However, a downward shift in the RCS signatures was observed as the angle of incidence further increased to θ-or-Φ = 60°, however, the tags RCS response is still detectable. This downward impact is increased when θ-or-Φ angles increased to 90°, along

from the tag. The tag's backscattered RCS responses are shown in Fig. 6, where each data bit B1, B2, B3 … B18 have 1:1 correspondence with resonators R_1, R_2, R_3 … R_{18}. From a data coding point

Fig. 9. (a) Electric current density on the surface of the tag when excited with horizontal plane waves at (a) 2.02 GHz, (b) 2.89 GHz, (c) 12.64 GHz, and (d) 3D reflected power pattern of the tag at 6.87 GHz.

with some vanishing RCS signatures. Because the incident EM field does not couple with into the slots when the tag is illuminated from the edge. Thus, at these angles (θ-or-$\Phi = 60$) some of the signatures disappear and some cause a reduction in the backscattering level.

The operation and physics of the proposed tag can be understood with the help of its surface current density and reflected power pattern, as shown in Figs 9(a)–9(d). The tag is excited by a horizontal plane wave from the z_+ direction at a 100 cm distance. Figure 9(a) shows that R_{18} has a surface current density of 0.35 A/m at 2.02 GHz, which is its resonance frequency. In the same way, using the resonance frequencies of 2.89 and 12.64 GHz which give a 0.669 and 0.05 A/m surface current density on their corresponding resonators R_{15} and spiral resonator (R_1), respectively. The higher current densities for their respective center resonance frequencies are showing a reflection of the plane wave by each resonator in the z_+ direction. Each resonator has a single resonance frequency at which it has maximum surface current density distribution, and the rest of the resonators have minimum surface current densities. Additionally, it has also been observed that the highest current distribution 0.669 A/m of R_{15} gives a higher spectral signature as compared to R_1 and R_{18},
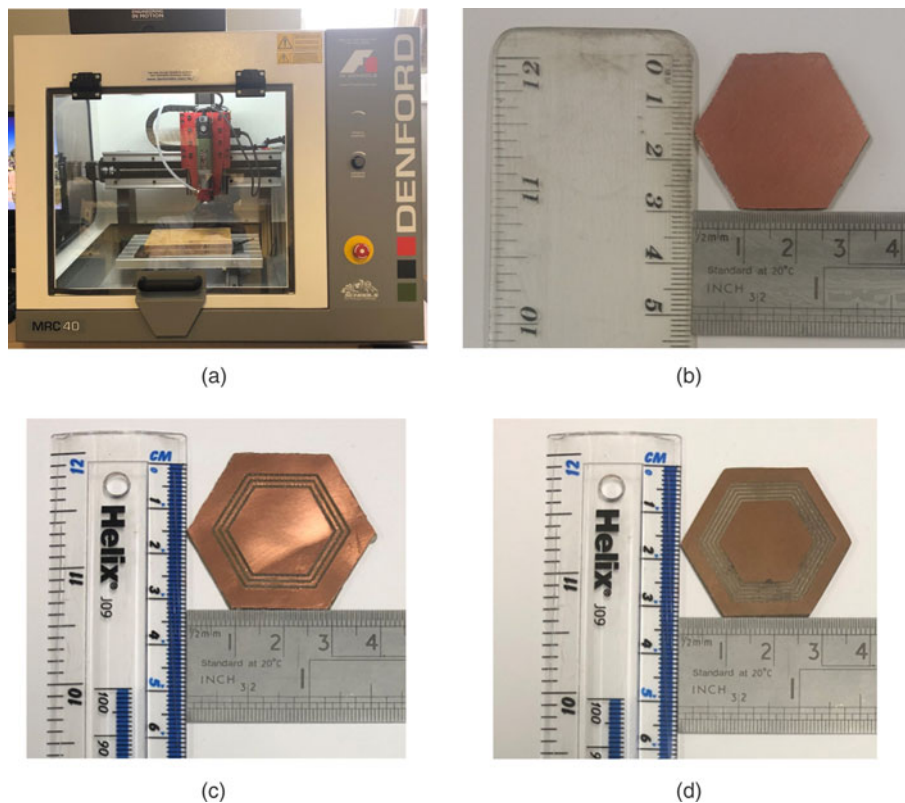
which means the higher surface current density will give a higher spectral signature. The far-field pattern of 3-D reflected power can be seen in Fig. 9(d), which gives a reflected power pattern in all "Φ" and "θ" angles at 6.87 GHz.

Code density

Chipless RFID tags store data in their geometrical structure that can be recovered (or decoded) through analysis of the received backscattered RF spectra resulting from an illuminating broadband RF source. In essence, the data stored are encoded in the tags' RCS [31]. In the past two decades, extensive research efforts have been reported on approaches to increase the code capacity and read range of chipless RFID tags [17]. For example, in [31] a tag with eight straight slots/resonators, producing eight corresponding frequency signatures in RCS is described; however, this tag is relatively large compared to its code density of 3.3-bits/cm^2; in [14], a 28.5-bit tag is reported with a high code density of 3.56-bits/cm^2; in [24], a 7.4-bits/cm^2 tag is reported, however, the tag's data can only be recovered in the near-field region of the tag. Tags may be categorized by their code density as reported by Munawar et al. in [14], which is a key parameter

Table 2. Comparison of proposed chipless RFID tag's code density, angular stability, and performance with the reported literature

Code density (bits/cm²)	Area (cm²)	Max read range	Capacity	Item encoding	Angular stability (Φ and θ)	Reference
0.25	16	Far-field	4 bits	Yes	No	[17]
2.5	2	Far-field	5 bits	Yes	No	[36]
2.74	3.65	Far-field	10 bits	Yes	$\Phi = 90°$	[37]
2.84	1.05	Far-field	3 bits	Yes	No	[8]
3.56	8	Far-field	28 bits	Yes	No	[14]
6	4	Far-field	24 bits	Yes	No	[22]
6.63	4.52	Far-field	30 bits	Yes	No	[26]
7.4	1.35	Near-field	10 bits	Yes	No	[24]
3.6	5.06	Far-field	18 bits	Yes	Θ and Φ up to 60°	This work

Fig. 10. (a) Denford milling machine used for tag manufacturing, (b) zero-slot tag, (c) two-slots tag, and (d) five-slots tag.

for comparing performance of tags, instead of analyzing various parameters such as dimension, code capacity, and operating frequency:

$$Code\ density = \frac{Code\ Capacity}{Tag\ Surface\ Area}$$

$$= \frac{Bits\ Encoded\ per\ Tag}{Surface\ Area} \quad (2)$$

Using equation (2), they claimed the highest code density of 3.56-bits/cm² [14]. Table 2 compares capacity, code density, maximum read range, item encoding, and angular stability achieved by various tags in the published literature to date. From these tags the highest code density achieved was 7.4-bits/cm² in [24] but its read range is limited to a few centimeters operating range. As it operates in the near-field region, it could not be used for tracking in biomass supply chain. In contrary, two other studies [22, 26] have reported a higher code density and readability in the far-field region, but they have very limited or no angular stability, and low RCS signature. This would be an issue in biomass-process supply chains, as the signals could easily be destroyed in the noisy environment. Therefore, the aim of the novel tag produced in this study was to be readable in the far field (maximum read range = 1800 cm), have maximum angular stability (up to θ-or-$\Phi = 60°$), providing high code density (3.6-bits/cm²), and have a high RCS signature in a compact size of 5.06 cm². Due to all these improvements in the tag designed geometry, the RCS signatures have significantly reduced the impact from the noisy biomass environment in comparison with similar studies [14, 17, 22, 24, 26, 31].
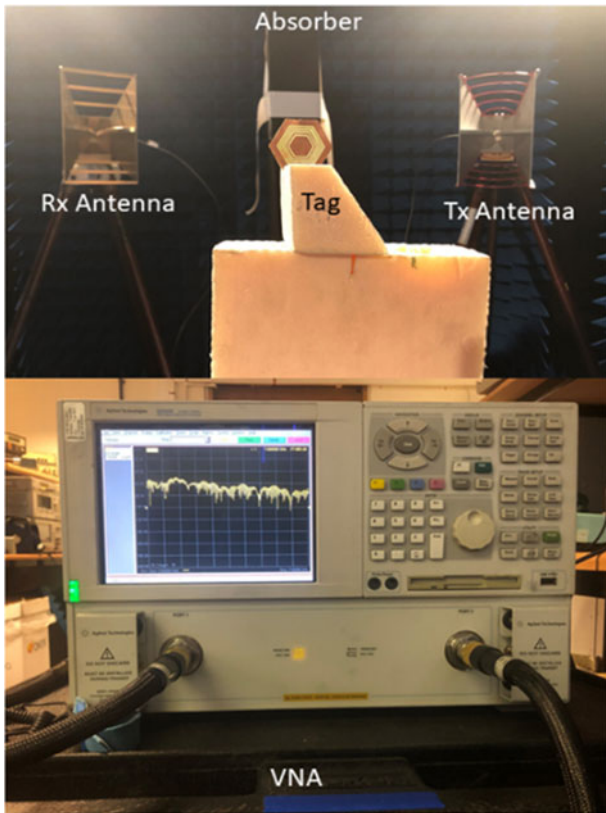
Fig. 11. Tag measurement made inside anechoic chamber with bistatic antennas, an absorber between them and manufactured tag is placed in front of antenna while VNA is placed outside.

Measurement setup

Three different coding combinations of the proposed tag have been manufactured on an FR4 substrate by using Denford milling machine at the University of Nottingham. The proposed tag could be easily manufactured by milling machine as the tag does not have a ground plane. The manufactured combinations are zero slot, two slot, and five slot tags, as shown in Fig. 10. Due to milling machine engraving limitation, a scaled-up version of the simulated tag was manufactured, where the slot size was scaled-up to 0.5 mm instead of 0.3 mm. The used FR4 PCB was received from RS with 0.035 mm thick copper cladding and 1.6 mm substrate depth.

To measure the RCS response of the manufactured tags, a bistatic antenna setup was used, as shown in Fig. 11. The setup consists of vector network analyzer (VNA) whose ports were connected to double-ridged horn antennas having 0.7–18 GHz bandwidth and 12 dBi gain. To achieve an accurate RCS response of the tag, the bistatic antennas and tag were placed inside an anechoic chamber while VNA was placed outside. One antenna was used as a transmitter (Tx) and the other was used as a receiver (Rx) and complex S_{21} (magnitude and phase) was measured as a function of frequency from the tag backscattering. The prepared tag was placed 60 cm away from two antennas. A calibration technique was used to remove the strong coupling effects between the antennas. The calibration consisted of capturing three different RCS measurements. First, an initial measurement of empty anechoic chamber without tag was conducted and referred to as $NoTagS_{21}$. Then, the second measurement was performed with equal-sized plate target with known S_{21} which is referred to as $RefTagS_{21}$. Finally, the desired tag was placed in front of the antennas and captured their
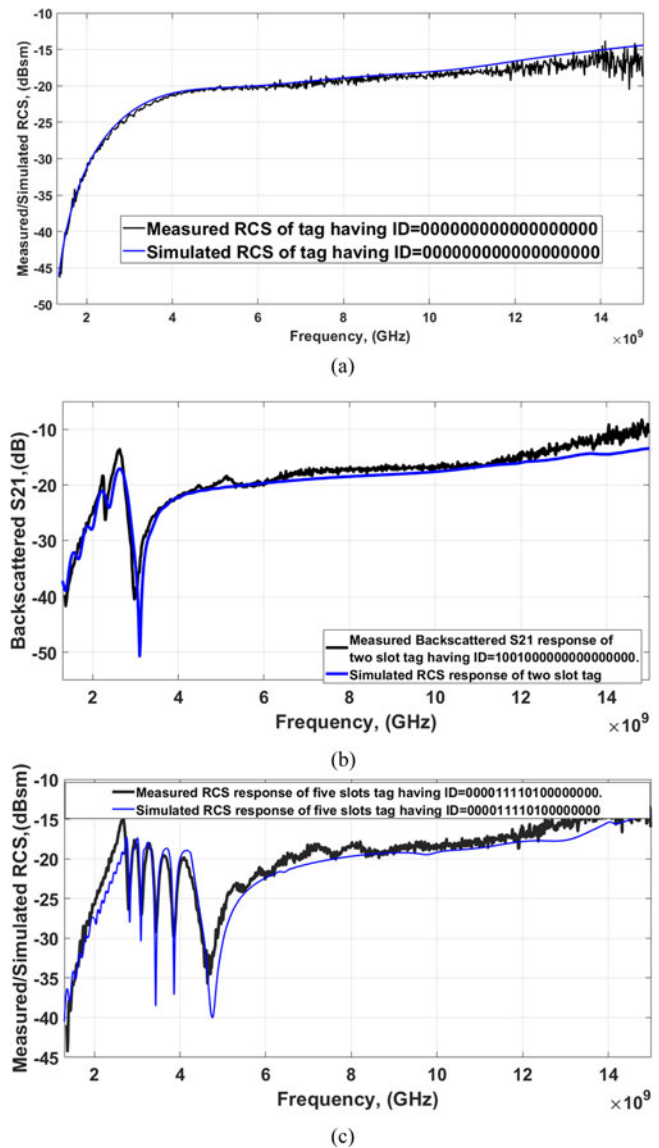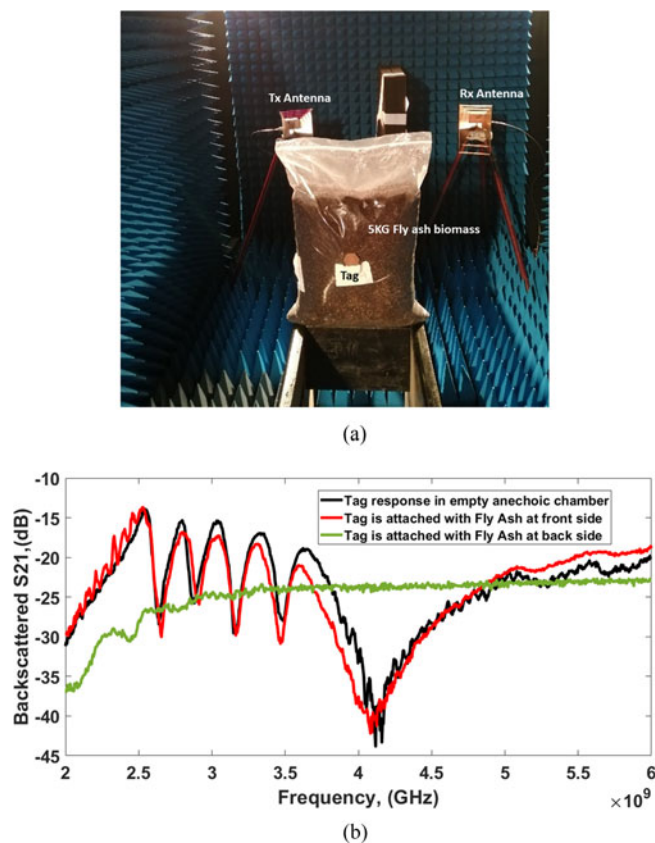

Fig. 12. Measured versus simulated RCS response of (a) zero-slot tag, (b) two-slots tag, and (c) five-slots tag.

reflections and referred to as $TagS_{21}$. The captured reflected data were processed in Matlab according to equation (3) for converting the backscattered S_{21} reflections to RCS. In equation (3), SimRCSPlate is the simulated response of $RefTagS_{21}$:

$$TagRCS = SimRCSPlate* TagS21 - NoTagS21 RefTagS21$$
$$- NoTagS21 2 \qquad (3)$$

Initially, a zero-slot tag was placed in front of the bistatic antenna setup and the backscattered S_{21} reflections were captured. The captured reflected data were processed in Matlab according to equation (3). Figure 12(a) shows the measured and simulated RCS of the zero-slot tag. The simulated and measured RCS responses of zero-slot tag were similar throughout the operating frequency band (1.5–15 GHz). The encoding data ID of this tag is 000000000000000000 (while the decimal value is "0"). The RCS responses of the two-slots tag were measured using the same

Fig. 13. (a) Tag is attached with fly ash at the front, back, and (b) the RCS response of tag only, tag attached at the front and back sides of biomass.

process of zero-slot tag. Figure 12(b) shows the measured and simulated RCS responses of the two-slots tag. The encoding data ID of this tag is 100100000000000000 (and the decimal value is "147456"). Figure 12(c) shows that the measured RCS response of five-slots tag, which is in good agreement with their corresponding simulated tag's RCS signatures. The data encoding ID of this tag is 0000011101000000000 (and the decimal value is "14848"). These experimental measurements suggest that the tag could be realized at industrial level, which could give $2^{18} = 262\,144$ different IDs for tracking and identifications purposes.

Practical implementation of the proposed tag

The aim of this research was to design a tag which could track the biomass supply chain at a different location during transportation. Additionally, the tag should be able to provide the biomass temperature and humidity level. To avoid self-heating of materials (biomasses) which leads to the decomposition of the material, formation of spores and fungus, and the release of flammable gases [5]. This can lead to fires and explosions in several parts of the biomass supply chain [6, 7]. This fire risk will be reduced by using proposed chipless RFID tags instead of battery-based tracking devices.

The proposed tag was attached to a 5 kg weight of fly-ash biomass and its backscattered S_{21} response was captured. The calibration setup elaborated in equation (3) was used with the addition of 5 kg fly-ash biomass. Initially, the tag was attached at the front of the fly ash and its RCS response was measured, as shown in Fig. 13. Figure 13 shows the tag only, tag attached at the front of the biomass, and at the back side of the biomass. A downward

shift in RCS spectral signatures was observed when the tag is attached at the front side of biomass. However, the tag response is still identifiable. In the next step, the tag is attached at the back side of 5 kg biomass. In this case the tag's spectral signatures disappeared, as shown in Fig. 13. Possibly the tag's backscattered signals could not penetrate through the dense volume of fly ash.

The future work of ongoing research is to find the maximum depth of tag reading inside bulk weight of biomass, monitoring temperature, and humidity level of different biomasses such as refuse-derived fuel, fly ash, rice husk, palm kernel shells, etc.

Conclusions

The design of a chipless RFID tag has been presented that is suitable for fabrication on a low-cost FR4 substrate and is suitable for tracking of biomass life cycle as it is easily disposed of during the fuel's combustion cycle. The tag design is further suited to fabrication on PET and Taconic TLX-0 substrates and using conducting materials that make it suited to fabrication by printing processes. The tag is compact and readable across a range of angles.

Three combinations namely zero slot, two slots, and five slots of the proposed tag's geometry were manufactured on the FR4 substrate by using Denford milling machine at the University of Nottingham. A bistatic antenna setup was used for capturing the tag's backscattered S_{21} signatures. The simulated and measured RCS signatures have strong agreement. The proposed tag was also tested with a 5 kg weight of fly-ash biomass.

The proposed tag will be further investigated to determine the maximum reading depth inside a bulk weight of biomass before increasing its measurement capability to include sensing ambient humidity, temperature, and CO_2 levels by using a fully passive chipless RFID tag. This would allow the prediction of environmental conditions that could have adverse or even disastrous effects during the transportation or storage of biomass fuels. The inclusion of such functionality is the subject of ongoing work.

References

1. Digest of UK Energy Statistics (DUKES) 2019 – GOV.UK. [Online]. Available at https://www.gov.uk/government/statistics/digest-of-uk-energy-statistics-dukes-2019 (Accessed 27 May 2020).
2. A burning issue: biomass is the biggest source of renewable energy consumed in the UK – Office for National Statistics. [Online]. Available at https://www.ons.gov.uk/economy/environmentalaccounts/articles/aburningissuebiomassisthebiggestsourceofrenewableenergyconsumedintheuk/2019-08-30 (Accessed 27 May 2020).
3. HARVESTING & COLLECTION. Tree felling systems.
4. **Ramírez Á, García-Torrent J and Tascón A** (2010) Experimental determination of self-heating and self-ignition risks associated with the dusts of agricultural materials commonly stored in silos. *Journal of Hazardous Materials* **175**, 920–927.
5. **Rentizelas AA, Tolis AJ and Tatsiopoulos IP** (2009) Logistics issues of biomass: the storage problem and the multi-biomass supply chain. *Renewable and Sustainable Energy Reviews* **13**, 887–894.
6. **Russo P, De Rosa A and Mazzaro M** (2017) Silo explosion from smoldering combustion: a case study. *Canadian Journal of Chemical Engineering* **95**, 1721–1729.
7. **Hedlund FH, Astad J and Nichols J** (2014) Inherent hazards, poor reporting and limited learning in the solid biomass energy sector: a case

study of a wheel loader igniting wood dust, leading to fatal explosion at wood pellet manufacturer. *Biomass and Bioenergy* **66**, 450–459.

8. **Amin EM, Saha JK and Karmakar NC** (2014) Smart sensing materials for low-cost chipless RFID sensor. *IEEE Sensors Journal* **14**, 2198–2207.

9. **Habib S, Ali A, Kiani GI, Ayub W, Abbas SM and Butt MFU** (2021) A low-profile FSS-based high capacity chipless RFID tag for sensing and encoding applications. *International Journal of Microwave and Wireless Technologies* **14**, 1–9.

10. **Ali A, Jafri SI, Habib A, Amin Y and Tenhunen H** (2017) RFID humidity sensor tag for low-cost applications. *Applied Computational Electromagnetics Society Journal* **32**, 176–184.

11. **Gilchrist A** (2016) *Industry 4.0: The Industrial Internet of Things*. New York, United States: Apress.

12. **Mo JPT, Sheng QZ, Li X and Zeadally S** (2009) RFID Infrastructure design: a case study of two Australian RFID projects. *IEEE Internet Computing* **13**, 14–21.

13. **Ibrahim A and Cumming DRS** (2011) Passive single chip wireless microwave pressure sensor. *Sensors and Actuators A: Physical* **165**, 200–206.

14. **Khan MM, Tahir FA, Farooqui MF, Shamim A and Cheema HM** (2016) 3.56-bits/cm^2 compact inkjet printed and application specific chipless RFID tag. *IEEE Antennas and Wireless Propagation Letters* **15**, 1109–1112.

15. ATEX and explosive atmospheres – Fire and explosion. [Online]. Available at https://www.hse.gov.uk/fireandexplosion/atex.htm (Accessed 27 May 2020).

16. Explosion Protection for Biomass, Wood Processing Plants – ATEX article – ATEXdb. [Online]. Available at https://www.atexdb.eu/atex_article/explosion-protection-for-biomass-wood-processing-plants (Accessed 27 May 2020).

17. **Feng Y, Xie L, Chen Q and Zheng L-R** (2015) Low-cost printed chipless RFID humidity sensor tag for intelligent packaging. *IEEE Sensors Journal* **15**, 3201–3208.

18. **Amin EM and Karmakar NC** (2012) Development of a low cost printable humidity sensor for chipless RFID technology, in 2012 *IEEE International Conference on RFID-Technologies and Applications* (RFID-TA), pp. 165–170.

19. **Vena A, Sydänheimo L, Ukkonen L and Tentzeris MM** (2014) A fully inkjet-printed chipless RFID gas and temperature sensor on paper, in 2014 *IEEE RFID Technology and Applications Conference* (RFID-TA), pp. 115–120.

20. **Amin EM and Karmakar N** (2011) Development of a chipless RFID temperature sensor using cascaded spiral resonators, in *Sensors, 2011 IEEE*, pp. 554–557.

21. **Amin EM, Bhuiyan S, Karmakar N and Winther-Jensen B** (2013) A novel EM barcode for humidity sensing, in 2013 *IEEE International Conference on RFID* (RFID), pp. 82–87.

22. **Javed N, Habib A, Amin Y, Loo J, Akram A and Tenhunen H** (2016) Directly printable moisture sensor tag for intelligent packaging. *IEEE Sensors Journal* **16**, 6147–6148.

23. **Preradovic S and Karmakar N** (2010) Chipless RFID tag with integrated sensor, in *Sensors, 2010 IEEE*, pp. 1277–1281.

24. **Herrojo C, Mata-Contreras J, Paredes F, Núñez A, Ramon E and Martín F** (2018) Near-field chipless-RFID tags with sequential bit reading implemented in plastic substrates. *Journal of Magnetism and Magnetic Materials* **459**, 322–327.

25. **Anum Satti J, Habib A, Anam H, Zeb S, Amin Y, Loo J and Tenhunen H** (2018) Miniaturized humidity and temperature sensing RFID enabled tags. *International Journal of RF and Microwave Computer-Aided Engineering* **28**, e21151.

26. **Noor T, Habib A, Amin Y, Loo J and Tenhunen H** (2016) High-density chipless RFID tag for temperature sensing. *Electronics Letters* **52**, 620–622.

27. **Vena A, Perret E, Tedjini S, Eymin Petot Tourtollet G, Delattre A, Garet F and Boutant Y** (2013) Design of chipless RFID tags printed on paper by flexography. *IEEE Transactions on Antennas and Propagation* **61**, 5868–5877.

28. **Vena A, Perret E and Tedjini S** (2011) Chipless RFID tag using hybrid coding technique. *IEEE Transactions on Microwave Theory and Techniques* **59**, 3356–3364.

29. **Vena A, Perret E and Tedjini S** (2012) Design of compact and auto-compensated single-layer chipless RFID tag. *IEEE Transactions on Microwave Theory and Techniques* **60**, 2913–2924.

30. **Vena A, Sydänheimo L, Tentzeris MM and Ukkonen L** (2015) A fully inkjet-printed wireless and chipless sensor for CO_2 and temperature detection. *IEEE Sensors Journal* **15**, 89–99.

31. **Dinesh R, Anila PV, Nijas CM, Sumi M and Mohanan P** (2014) Modified open stub multi-resonator based chipless RFID tag, in 2014 *XXXIth URSI General Assembly and Scientific Symposium* (URSI GASS), pp. 1–4.

32. **Catarinucci L, Colella R and Tarricone L** (2013) Enhanced UHF RFID sensor-tag. *IEEE Microwave and Wireless Components Letters* **23**, 49–51.

33. **Preradovic S and Karmakar NC** (2009) Design of fully printable planar chipless RFID transponder with 35-bit data capacity, in 2009 *European Microwave Conference* (EuMC), pp. 13–16.

34. **Ma Z and Jiang Y** (2019) High-density 3D printable chipless RFID tag with structure of passive slot rings. *Sensors* **19**, 2535.

35. **CST Studio Suite 3D EM simulation and analysis software**. [Online]. Available at https://www.3ds.com/products-services/simulia/products/cst-studio-suite/ (Accessed 12 May 2020).

36. **Amin EM, Karmakar NC and Jensen BW** (2016) Fully printable chipless RFID multi-parameter sensor. *Sensors and Actuators A: Physical* **248**, 223–232.

37. **Jabeen I, Ejaz A, Akram A, Amin Y, Loo J and Tenhunen H** (2019) Elliptical slot based polarization insensitive compact and flexible chipless RFID tag. *International Journal of RF and Microwave Computer-Aided Engineering* **29**, e21734.

Amjad Ali is currently pursuing Ph.D. in electrical and electronics engineering from the Department of Electrical Engineering at the University of Nottingham, UK. His research interest is designing chipless RFID tags for tracking biomass pellets supply chain and -monitoring their ambient humidity, temperature, and CO_2 level. He joined GGIEMR Research group in 2018 at the University of Nottingham, UK.

Christopher Smartt obtained MEng and Ph.D. in electrical and electronic engineering from the University of Nottingham in 1991 and 1995, respectively. Smartt worked on simulation of microwave devices for 2 years as a research assistant at the University of Nottingham and later he joined BAE SYSTEMS where he worked on 2D and 3D full-field time and frequency-domain finite-element techniques for electromagnetic field simulation in aerospace applications. In 2007 he re-joined the George Green Institute for Electromagnetics Research at the University of Nottingham as a research fellow where his research interests include the development and application of computational electromagnetics methods and the development of electromagnetic field measurement techniques including time-domain and near-field methods, with applications to EMC and EMI studies.

Professor Ed Lester Ed started out as Marine Chemist as an undergraduate before taking on a PhD in Chemical Engineering. Since then he has been busy working at the interface between chemistry and engineering. His PhD focussed on the use of image analysis to characterise fuels and predict their combustion performance. These techniques are still used by power generators around the world to inform procurement decisions as well as forensic analysis of boiler issues. Ed successfully used novel image analysis techniques to solve a key issue that had hampered the development of continuous supercritical fluid reactors. This breakthrough led to the development of new reactor designs and various patent filings. Promethean Particles Ltd was formed at the end of 2007 to exploit this new intellectual property and the company now operates the worlds largest continuous supercritical water system for the production of nanomaterials. The company makes and sells nanomaterials to clients around the world, from Japan to USA. He founded Promethean Particles at the end of 2007.

Dr. Orla Williams is an Anne McLaren Research Fellow at the University of Nottingham investigating sustainable biomass-based processing techniques to produce critical raw materials for the circular economy. She has graduated from the University of Bath with an MEng in mechanical engineering and has an Engineering Doctorate (EngD) in chemical and environmental engineering from the University of Nottingham. She is also a chartered engineer (CEng) with the Institution of Mechanical Engineers (IMechE) with several years of experience in the transport, construction, and power generation sectors.

Steve Greedy was born in Cardiff, UK. He earned MEng and Ph.D. degrees in 1998 and 2002 from the University of Nottingham. He is an associate professor within George Green Institute for Electromagnetics Research. His interests are in the area of experimental and computational electromagnetics with a focus on techniques used in the study of electromagnetic compatibility and signal integrity, specifically mechanisms that impact performance, and coexistence of wired and wireless communication systems.